**OPEN**

# Microwave magnetic field modulation of spin torque oscillator based on perpendicular magnetic tunnel junctions

Witold Skowroński[1*], Jakub Chęciński[1], Sławomir Ziętek[1], Kay Yakushiji[2] & Shinji Yuasa[2]

Modulation of a microwave signal generated by the spin-torque oscillator (STO) based on a magnetic tunnel junction (MTJ) with perpendicularly magnetized free layer is investigated. Magnetic field inductive loop was created during MTJ fabrication process, which enables microwave field application during STO operation. The frequency modulation by the microwave magnetic field of up to 3 GHz is explored, showing a potential for application in high-data-rate communication technologies. Moreover, an inductive loop is used for self-synchronization of the STO signal, which after field-locking, exhibits significant improvement of the linewidth and oscillation power.

Spin-transfer-torque nano oscillators based on both fully-metallic multilayers[1] and magnetic tunnel junctions (MTJ)[2] are widely studied due to their potential applications in future wireless communication[3] and magnetic recording[4]. Up to now, the most promising parameters in terms of oscillation power and linewidth have been measured for MTJs with an in-plane magnetized reference layer and perpendicularly magnetized free layer[5,6], which also enable magnetic-field-free operation[7,8]. To further enhance spin torque oscillator (STO) characteristics, phase-locking to another STO[9] or external microwave signals[10] were suggested. Recently, electronic phase-lock loops (PLL) using uniform precession mode oscillations[11] and magnetic vortex[12] have been presented. In addition, self-synchronization via a field loop was shown in the in-plane magnetized MTJs[13].

Another important feature of STO is the ability to tune the oscillation frequency over wide range, which is essential for wireless communication devices. Precession frequency of operating STO depends on the bias current due to its inherent nonlinear nature[14], which is used in the aforementioned PLL circuits. Various modulation techniques presented in uniformly precessing MTJs[15,16] and vortex-based oscillators[17] were shown; however, an even stronger dependence of the STO frequency on an external magnetic field is expected, which would allow for higher modulations rates, as numerically predicted in ref. [18]. MTJs with an additional magnetic field line were already tested for STO-based read head sensors with a transition time down to 2-ns[19].

In this work, we present an experimental study of STO based on an MTJ with a perpendicularly magnetized free layer. In contrast to the vortex based STO[20], we use a uniform oscillation mode of the free layer, which is characterized by higher oscillation frequencies. An additional, isolated microwave line was fabricated on the top of the MTJ, which enables microwave magnetic field application during STO operation. At optimal configuration (static magnetic field, current bias), the STO operation frequency of $f = 5\,GHz$ and linewidth $\delta f = 10\,MHz$ were measured, which enables field-modulation at the rate of up to 3 GHz. Moreover, after injecting the amplified STO signal to the field line, and creating so-called inductive feedback loop, we observed the quality factor improvement to $Q > 18000$; however, at the cost of bringing the system to the edge of stability.

## Results

Vibrating sample magnetometry (VSM) measurements are presented in Fig. 1(a). Due to a significant contribution of a double CoFeB/MgO interface to the magnetic anisotropy of the top free layer, the saturation field value in perpendicular orientation is $H_K = 1.2\,kOe$, indicating effectively weak in-plane magnetic anisotropy. After the nanofabrication process, the demagnetizing field in the perpendicular direction decreases, which leads to an

[1]AGH University of Science and Technology, Department of Electronics, Al. Mickiewicza 30, 30-059, Kraków, Poland. [2]National Institute of Advanced Industrial Science and Technology (AIST), Spintronics Research Center, Tsukuba, Ibaraki, 305-8568, Japan. *email: skowron@agh.edu.pl
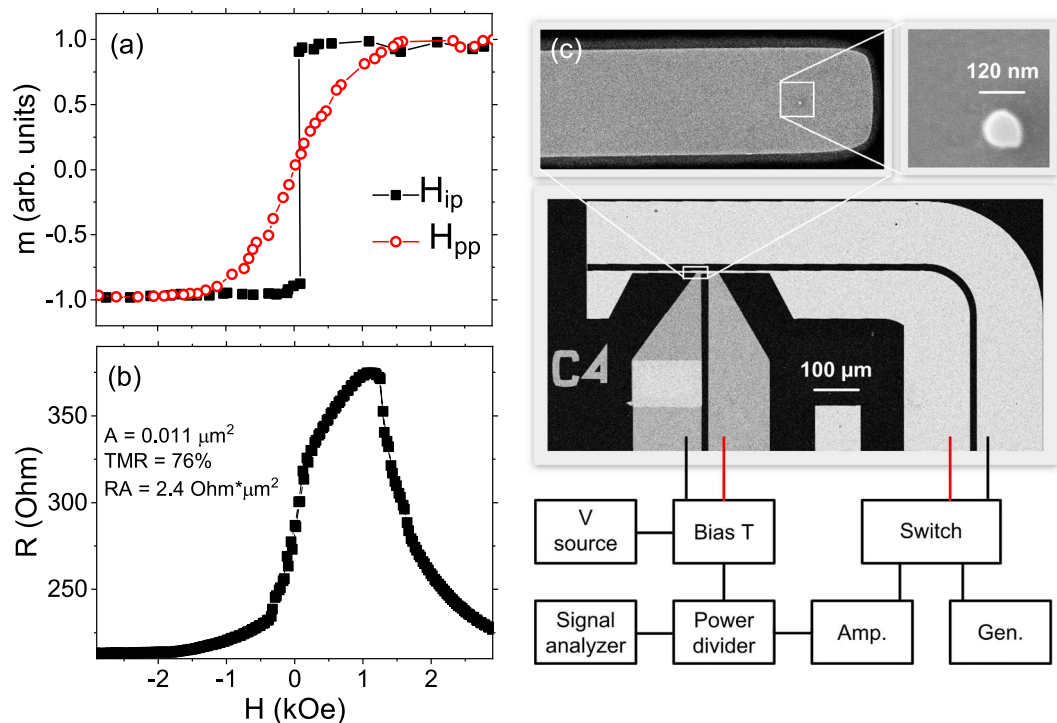
**Figure 1.** (**a**) Magnetization loops measured in the magnetic field applied in the sample plane $H_{ip}$ and perpendicular to the sample plane $H_{pp}$, (**b**) resistance vs. in-plane magnetic field loop of a fabricated MTJ, (**c**) micrograph of the device (the top two images were recorded during the fabrication process) with a schematic representation of the measurement setup.

effective perpendicular anisotropy of the free layer of the patterned device - Fig. 1(b). The TMR ratio reaches 76% with the RA product of $2\,\Omega \times \mu m^2$.

After application of a negative bias voltage, indicating electron flow from the top free layer to the bottom reference layer, i.e., destabilization of the parallel magnetization alignment, the STO signal is measured in the presence of an external magnetic field. An example of the auto-oscillation signal measured in a magnetic field applied at $\theta = 65°$ with respect to the sample plane is presented in Fig. 2(a). For selected amplitudes of magnetic field, the linewidth at half maximum drops to around 10 MHz, resulting in a quality factor of several hundreds. We note that the STO signal is present for a range of $\theta$ between 50 and 90°, which varies slightly between devices. An example STO signal vs. bias current dependence is presented in Fig. 2(b), together with the STO frequency and power (expressed in dB over noise floor) - Fig. 2(c). Reversing the bias polarity results in a much weaker STO signal and broader linewidth (not shown), similarly to other reports[21].

Next, we explore the magnetic field modulation possibilities of the STO signal. The magnetic field was kept constant $H = 2\,kOe$ at $\theta = 65°$, resulting in auto-oscillations at around 5.7 GHz. After applying an rf signal of frequency $f_{MOD}$ to the magnetic field line, modulation sidebands are clearly visible; however, only the frequencies below the main peak - Fig. 3(a). The modulation power was set to $P_{MOD} = 0\,dBm$. Single sideband modulation has been recently observed in a current-driven STO and such behaviour was explained by the non-linear dependence of the frequency and power on bias voltage[22]. Strikingly, in our case a clear modulation signal was observed up to $f_{MOD} = 3\,GHz$, which exceeds frequency modulation range reported to date in the in-plane magnetized MTJs.

To further elucidate on the microwave field-modulated STO behaviour, we repeated the frequency spectrum measurements for increased $P_{MOD}$. Figure 3(b) present the $f_{MOD}$ vs. frequency map for increased $P_{MOD} = 10\,dBm$. In contrast to the measurement performed at $P_{MOD} = 0\,dBm$, where a linear dependence of the sideband and modulation frequency is measured, an increased modulation power results in the main peak frequency deviation from its original position, determined by the bias current and magnetic field. We ascribe this effect to the injection-locking of the STO to higher harmonics of the modulating signal[23,24].

In order to exclude possible modulation mechanism via bias current that is induced in a neighbouring supply line from the magnetic field line, the modulation signal was also connected directly to the bias-tee via radio-frequency combiner in a separate experiment. In this case, the modulation signal was also measured, but only up to $f_{MOD} = 1.2\,GHz$, which is well below the field-modulated range that exceeds 3 GHz - Fig. 4(a,b).

To reproduce the observed effect theoretically, macrospin simulation were performed. The parameters of the system were chosen to follow the experimental values whenever possible and were as following: $\mu_0 M_s = 1.6\,T$, maximum effective anisotropy field 300 Oe, damping constant $\alpha = 0.01$, junction diameter 120 nm, free layer thickness 1.8 nm. The reference layer magnetization was assumed to be fixed in the sample plane and the small effective dipolar field originating from bottom parts of the stack was included in the free layer. The Landau-Lifshitz-Gilbert-Slonczewski equation was integrated numerically, assuming an angular dependence
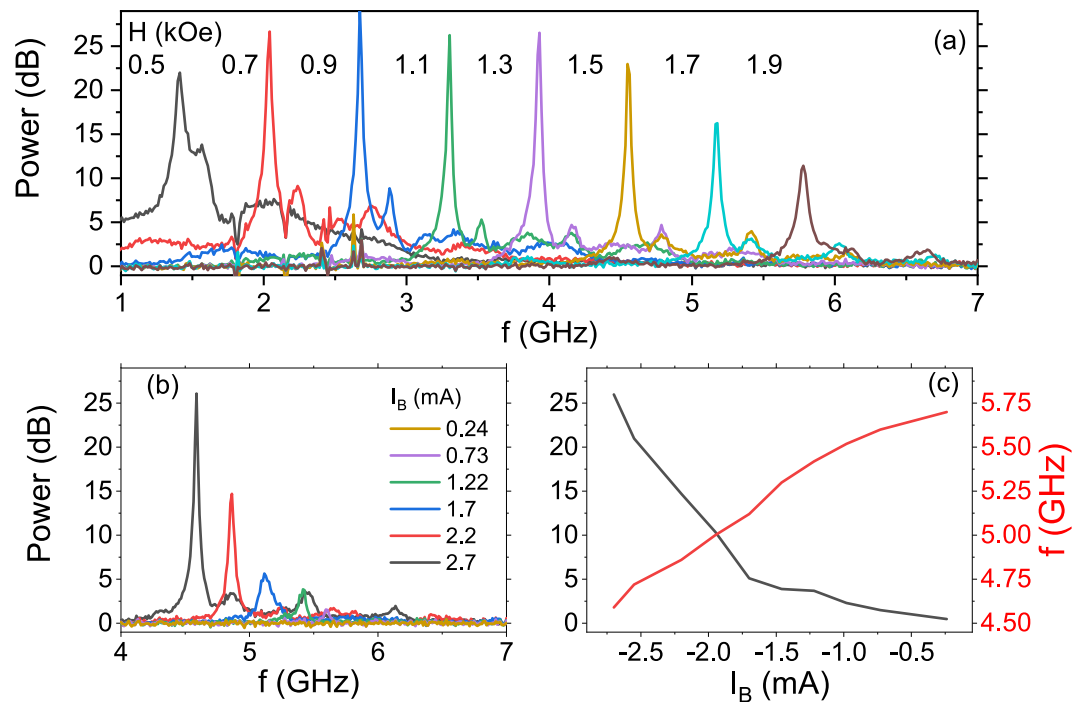
**Figure 2.** (**a**) STO power (expressed in dB over the noise floor) measured in different magnetic fields applied at 65° with respect to the sample plane, (**b**) bias current dependence on the STO signal. The STO frequency and power extracted from (**b**) are presented as a function of the bias current (**c**).
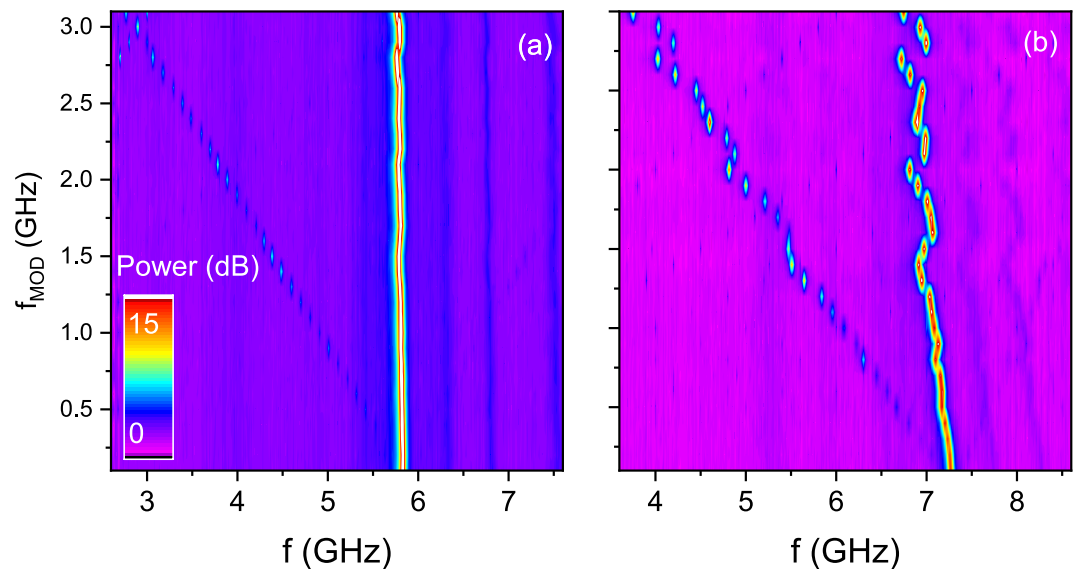


**Figure 3.** STO signal with field-modulation of $f_{MOD}$ up to 3 GHz and $P_{MOD} = 0$ dBm (**a**) and $P_{MOD} = 10$ dBm (**b**). Deviation from the main STO peak is present for higher modulation power.

of the spin torque term with the angular term $\lambda^{5,25}$ equal to approximately 0.69. By applying a bias current of −2.05 mA and an external magnetic field of 2.2 kOe at $\theta = 85°$, we were able to obtain stable oscillations at a frequency similar to the one presented in Fig. 4(a,b). Next, we performed a set of simulations for two different modulation approaches: one driven by the external magnetic field - Fig. 4(c), and one driven by the bias current - Fig. 4(d). Clearly, the modulation rate is significantly stronger in the case of the magnetic field modulation, further supporting the conclusion obtained from the experiment.

Finally, auto-synchronization of the STO with a feedback loop was explored. The microwave STO signal was amplified and fed to the inductive magnetic field line. The dependences of the STO power on the magnetic field without and with the feedback loop are presented in Fig. 5(a,b). Without a feedback connected, the STO power reaches 25 dB over noise floor and monotonically decreases with increasing magnetic field. In the case of the
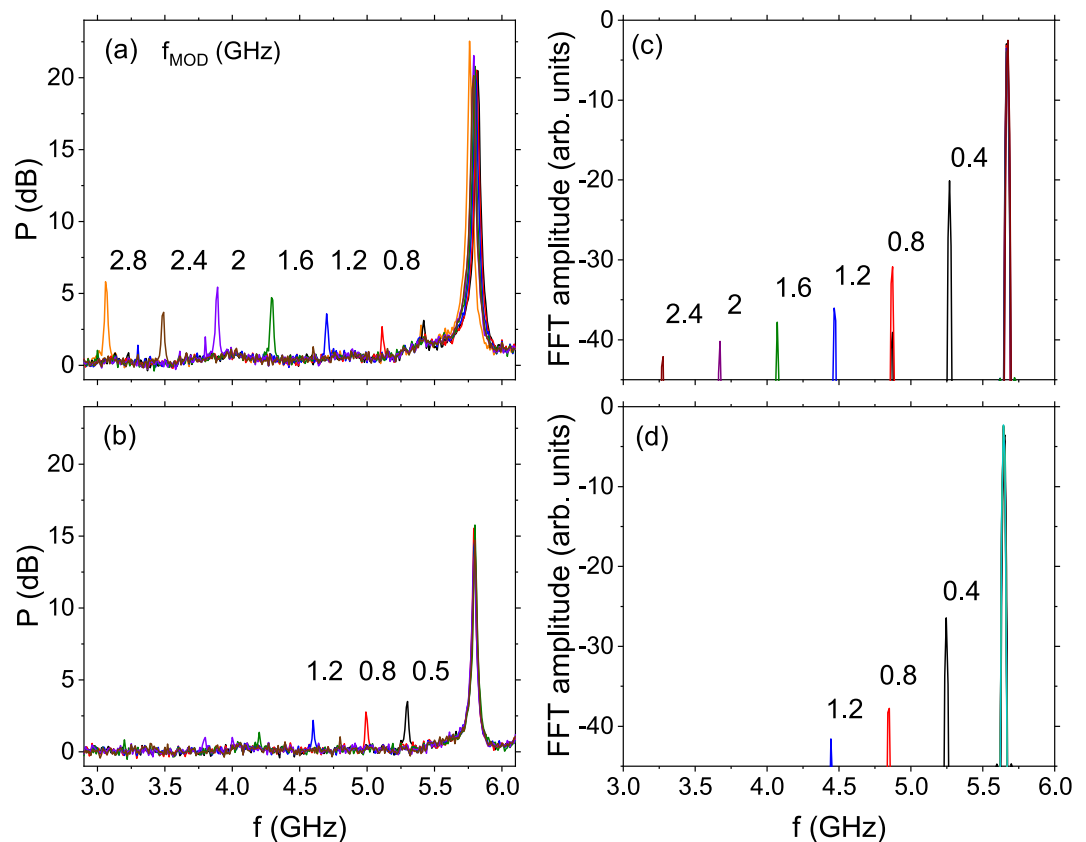
**Figure 4.** Comparison between magnetic field modulation (**a**) and current bias modulation (**b**) indicating higher modulation rate for Oersted field method, as predicted in[15]. Corresponding macrospin simulation results are presented in (**c**) and (**d**).

feedback-STO, apart from the main peak, several side-peaks are visible in each spectrum. The distance (in the frequency domain) between peaks is fixed to around 0.2 GHz, which is a result of delay caused by the total feedback line length of around 1.5 m. The measured amplitude of each peak increases when the free-running oscillations frequency at a given bias and magnetic field corresponds to the resonance frequency of the feedback loop. This results in an increased oscillations power up to 30 dB with respect to the STO without a feedback. An example showing one of the strongest STO signals measured with the feedback loop is presented in Fig. 5(c). We note that the positive feedback used in the circuit design may cause the system to be at the stability limit, i.e., further increase in gain of the amplifier may case self-excitation of the circuit even without STO presence. Nevertheless, the obtained STO Q factor of above 18000 and the oscillation power spectral density reaching 25 nV/$\sqrt{Hz}$ are promising for future applications.

In conclusion, the STO properties of the magnetic tunnel junction with perpendicularly magnetized free layer were investigated in the presence of an additional microwave magnetic field. Application of the external field enabled STO frequency modulation up to 3 GHz, which exceeds the limit for the bias-current modulation methods. By connecting the inductive field line to the amplified STO signal and creating a feedback loop, greater power and a Q-factor of up to 18000 were obtained.

## Methods

Multilayer of the following structure: Ru(4)/IrMn(6)/CoFe(2.5)/Ru(0.8)/CoFeB(2.5)/MgO (1)/CoFeB(1.8)/ MgO(1)/Ru(3)/Ta(5)/Ru(2)/Pt(3) (thickness in nm) was deposited on chemically-mechanically polished Si wafer using magnetron sputtering method. The bottom CoFeB is pinned to the synthetic antiferromagnetic structure and acts as an in-plane magnetized reference layer. The magnetic properties of the films were determined using VSM. MTJ devices were fabricated using electron beam lithography, ion-beam milling and lift-off processes into circular and elliptical nanopillars of diameters ranging from 120 to 450 nm, with the additional field line, separated from the top and bottom contact by a 100-nm thick $Al_2O$ layer. Electrical contacts and the field line was made of Al(20)/Au(30) conducting layer. The micrograph of the MTJ design is presented in Fig. 1(c).

Electrical transport properties were determined in the rotating probe station enabling magnetic field application at an arbitrary angle with respect to the MTJ axis. Custom design microwave, five-tip probe (T-Plus) was used to connect a bias source (Keithley 2401) and signal analyser (Agilent PXA N9030A) via broadband bias-T (Mini Circuits ZX86-12G) to the MTJ. An external radio-frequency (rf) signal (Agilent E8257D) was fed to the field line using the same microwave probe. Alternatively, the amplified (Mini circuits ZVA-213, 26 dB Gain) STO
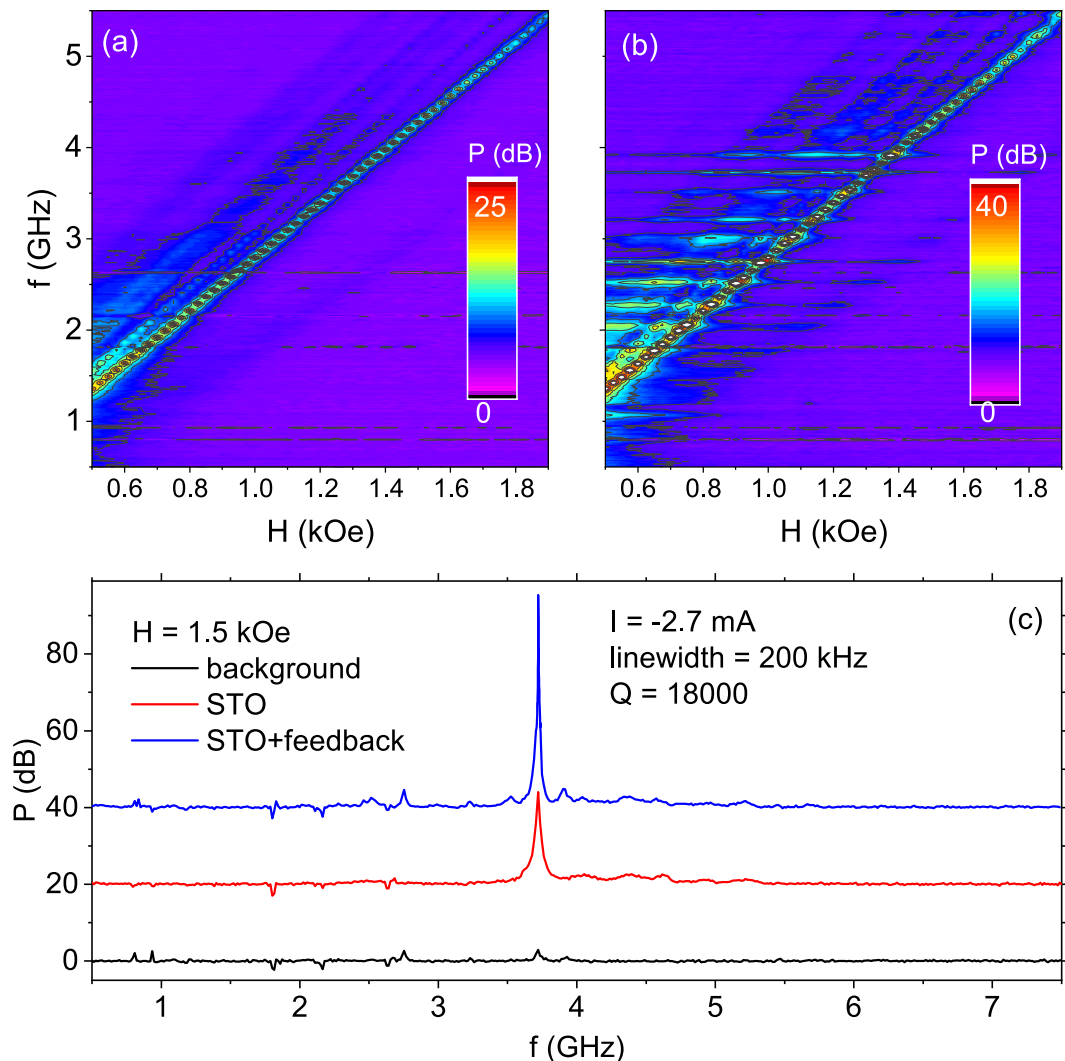
**Figure 5.** STO performance with an inductive feedback-loop. Oscillations frequency vs. magnetic field applied in the $\theta = 65°$ recorded without (**a**) and with (**b**) the feedback loop connected. Horizontal lines in (**b**) represents the inverse of feedback loop delay of around $0.2\,\mathrm{GHz}$. (**c**) Example STO plots with the feedback loop turned off and on together with a background signal. Curves are offset by $20\,\mathrm{dB}$ for clarity.

signal was connected to field line via broadband power divider (Mini Circuits ZN2PD2-63). Transport and rf properties were determined in ten different devices exhibiting qualitatively similar results.

In addition, static transport measurements were performed in a perpendicular magnetic field using the four-point method on different MTJs fabricated on the same wafer, in order to extract the resistance area (RA) product and the tunnelling magnetoresistance (TMR) ratio.

## References

1. Tsoi, M. *et al.* Generation and detection of phase-coherent current-driven magnons in magnetic multilayers. *Nature* **406**(6791), 46–48 (2000).
2. Deac, A. M. *et al.* Bias-driven high-power microwave emission from MgO-based tunnel magnetoresistance devices. *Nature Physics* **4**(10), 803 (2008).
3. Chen, T. *et al.* Spin-torque and spin-hall nano-oscillators. *Proceedings of the IEEE*, 104(10):1919–1945 (Oct 2016).
4. Braganca, P. M. *et al.* Nanoscale magnetic field detection using a spin torque oscillator. *Nanotechnology*, 21(23):235202, (may 2010).
5. Taniguchi, T. *et al.* Critical field of spin torque oscillator with perpendicularly magnetized free layer. *Applied Physics Express*, 6(12):123003, (dec 2013).
6. Maehara, H. *et al.* Large emission power over 2 uw with high Q factor obtained from nanocontact magnetic-tunnel-junction-based spin torque oscillator. *Applied Physics Express*, 6(11):113005, (November 2013).
7. Skowroński, W., Stobiecki, T., Wrona, J., Reiss, G. & van Dijken, S. Zero-field spin torque oscillator based on magnetic tunnel junctions with a tilted CoFeB free layer. *Applied Physics Express* **5**(6), 063005 (2012).
8. Zhongming Zeng *et al.* Ultralow-current-density and bias-field-free spin-transfer nano-oscillator. *Scientific Reports* **3**(Mar), 1426 (2013).

9. Shehzaad Kaka *et al*. Mutual phase-locking of microwave spin torque nano-oscillators. *Nature* **437**(7057), 389–392 (2005).
10. Hanuman Singh, A. *et al*. Self-injection locking of a spin torque nano-oscillator to magnetic field feedback. *Phys. Rev. Applied* **10**(Aug), 024001 (2018).
11. Tamaru, S., Kubota, H., Yakushiji, K., Yuasa, S. & Fukushima, A. Extremely coherent microwave emission from spin torque oscillator stabilized by phase locked loop. *Scientific Reports* **5**(Dec), 18134 (2015).
12. Martin Kreissig, R. *et al*. Vortex spin-torque oscillator stabilized by phase locked loop using integrated circuits. *AIP Advances* **7**(5), 056653 (2017).
13. Dinesh Kumar, K. *et al*. Coherent microwave generation by spintronic feedback oscillator. *Scientific Reports* **6**(Aug), 30747 (2016).
14. Slavin, A. & Tiberkevich, V. Nonlinear auto-oscillator theory of microwave generation by spin-polarized current. *IEEE Transactions on Magnetics*, 45(4):1875–1918, (April 2009).
15. Ruiz-Calaforra, A. *et al*. Frequency shift keying by current modulation in a mtj-based stno with high data rate. *Applied Physics Letters* **111**(8), 082401 (2017).
16. Muduli, P. K. *et al*. Nonlinear frequency and amplitude modulation of a nanocontact-based spin-torque oscillator. *Phys. Rev. B* **81**(Apr), 140408 (2010).
17. Manfrini, M. *et al*. Frequency shift keying in vortex-based spin torque oscillators. *Journal of Applied Physics* **109**(8), 083940 (2011).
18. Purbawati, A., Garcia-Sanchez, F., Buda-Prejbeanu, L. D. & Ebels, U. Enhanced modulation rates via field modulation in spin torque nano-oscillators. *Applied Physics Letters* **108**(12), 122402 (2016).
19. Nagasawa, T., Suto, H., Kudo, K., Mizushima, K. & Sato, R. Frequency transition of spin-torque oscillator under the magnetic-field pulse in nanosecond range. *Journal of Applied Physics* **109**(7), 07C907 (2011).
20. Sumito Tsunegi *et al*. Self-injection locking of a vortex spin torque oscillator by delayed feedback. *Scientific Reports* **6**(May), 26849 EP (2016).
21. Ewa Kowalska *et al*. Tunnel magnetoresistance angular and bias dependence enabling tuneable wireless communication. *Scientific Reports* **9**(1), 9541 (2019).
22. Raghav Sharma *et al*. A high-speed single sideband generator using a magnetic tunnel junction spin torque nano-oscillator. *Scientific Reports* **7**(1), 13422 (2017).
23. Urazhdin, S., Tabor, P., Tiberkevich, V. & Slavin, A. Fractional synchronization of spin-torque nanooscillators. *Phys. Rev. Lett.* **105**(Aug), 104101 (2010).
24. Hanuman Singh, K. *et al*. Integer, fractional, and sideband injection locking of a spintronic feedback nano-oscillator to a microwave signal. *Phys. Rev. Applied* **8**(Dec), 064011 (2017).
25. Hitoshi Kubota *et al*. Spin-torque oscillator based on magnetic tunnel junction with a perpendicularly magnetized free layer and in-plane magnetized polarizer. *Applied Physics Express* **6**(10), 103003 (2013).

## Acknowledgements

## Author contributions

K.Y. and S.Y. performed sample deposition and carried out VSM measurements, S.Z. and W.S. designed the device layout and carried out nanostructurization process, W.S. performed transport and rf measurements, J.Ch. performed macrospin simulations. W.S. wrote the manuscript with an input of J.Ch. All authors reviewed the manuscript.

## Competing interests

The authors declare no competing interests.

## Additional information

**Correspondence** and requests for materials should be addressed to W.S.

**Reprints and permissions information** is available at www.nature.com/reprints.

**Publisher's note** Springer Nature remains neutral with regard to jurisdictional claims in published maps and institutional affiliations.